Unveiling the Origin of Third Harmonic Generation in Hybrid ITO-Plasmonic Crystals

Aouani, Heykel; Navarro-Cia, Miguel; Rahmani, Mohsen; Maier, Stefan A.

DOI:
10.1002/adom.201500112

DOI: 10.1002/((adom.201500112))
Article type: Communication

Unveiling the Origin of Third Harmonic Generation in Hybrid ITO-Plasmonic Crystals

*Heykel Aouani**[†], Miguel Navarro-Cía[†], Mohsen Rahmani, and Stefan A. Maier*

[†]Heykel Aouani and Miguel Navarro-Cía contributed equally to this work

Dr. H. Aouani, Dr. M. Rahmani, Prof. S. A. Maier
The Blackett Laboratory, Department of Physics, Imperial College London, London SW7 2AZ, United Kingdom
E-mail: h.aouani@imperial.ac.uk
Dr. M. Navarro-Cía
Optical and Semiconductor Devices Group, Department of Electrical and Electronic Engineering, Imperial College London, London SW7 2BT, United Kingdom

Keywords: plasmonic crystal, hybrid plasmonic antenna, nonlinear nanophotonics, third harmonic generation, spectral analysis

The advent of novel lithographic techniques enabling the shaping of noble metals at the nanoscale is offering unprecedented opportunities for generating and manipulating light within subwavelength regions[1-3]. In recent years, the development of functional nanoscale elements such as plasmonic antennas, transducers between free radiation and localized energy[4,5], has led to major advances in various research fields including single molecule detection[6-8], directive nanosources of light[9-11], vibrational spectroscopy[12-14] and nonlinear interactions at the nanoscale[15-17]. For the latter, while the enhanced local fields created by plasmonic structures can be exploited for upconverting light at the nanoscale and for ultrafast processing of optical signals[18-19], their opacity prevents exploiting phase matching in order to reach high nonlinear emission, which severely limits their practical use. Therefore, the development of nanoscale devices exhibiting stronger nonlinear responses is highly required for proposing future efficient integrated nanophotonic components.

One promising strategy for reaching higher nonlinear nanoscale responses is related to the integration of an active nonlinear medium in the near field of a plasmonic structure. Indeed, while most works in nonlinear nanophotonics have focused on intrinsic responses from pure

metallic nanostructures, few recent studies have investigated the extrinsic responses from nonlinear materials localized in the vicinity of plasmonic devices[20-22]. In particular, hybrid nanostructures made by a mix of polymer or semiconductor and metallic materials have been recently proposed for enhancing nonlinear interactions between light and nanoscale elements[22-25]. Here, we propose a hybrid plasmonic crystal defined by a periodic arrangement of gold and indium tin oxide (ITO) materials for efficient frequency tripling of infrared light. We demonstrate that higher third harmonic generation (THG) conversion efficiency can be reached with the hybrid crystal compared to its bare plasmonic configuration, and that the origin of the nonlinear enhancement is related to the semiconductor material. Indeed, we introduce a new characterization method for unambiguously tracing the origin of the nonlinear signal in hybrid plasmonic systems, thus opening new avenues for identifying, understanding and optimizing nonlinear responses in complex mixed media.

All plasmonic nanostructures presented in this work were fabricated by a combination of etch-down and lift-of methods. Briefly, sputtering deposition was used to cover a quartz substrate with a 40 nm ITO film. The ITO film was attested to be a heavily-doped n-type semiconductor. Arrays of ITO nanodots (diameter between 25 and 35 nm) were fabricated by combining e-beam lithography and ion beam etching. The gold nanorods shapes were then defined around the ITO nanodots and a final lift-off step leads to the hybrid or bare plasmonic crystals presented in **Figure 1a,b**. ITO was chosen as nonlinear active medium for the hybrid plasmonic crystal due to its high intrinsic third order susceptibility[26].

The linear properties of both crystals were investigated numerically with a full-wave finite-difference time-domain (FDTD) technique (see Experimental Section for more details). The crystals were modelled using a symmetric unit cell with dimensions in accordance to the SEM pictures of Figure 1a,b. The intensity enhancement maps at the *xy* cross-section plane of the unit cell (**Figure 1c,d**) for the wavelength of the peak in the reflectance (**Figure 1e**) were

recorded to be used in the discussion. Simply notice now that the largest intensity is observed within the gaps and that the intensity in the metal resembles a horizontal hourglass with decreasing/increasing values toward the *x/y* edges.

The experimental linear characterization of the hybrid and bare plasmonic crystals was performed by Fourier-transform infrared spectroscopy (FTIR, Bruker Hyperion 2000). The corresponding extinction spectra (defined as 1-transmission) are presented in **Figure 1f**. A slight red-shift of the resonance peak position is observed for both configurations compared to the numerical predictions of Figure 1e, which can be attributed to minor defects related to the fabrication process (as-deposited material properties, thickness of the gold layer, roughness...), but the shapes of the measured extinction cross sections agree well with the simulated spectra. We point out that the crystal arrangement significantly changes the lifetime of the system, leading to a broadening of the plasmonic resonance compared to the corresponding isolated nanodimer studied later on (see Supplementary Information for more discussion).

We started our nonlinear investigations by measuring the third harmonic spectra from the hybrid and bare plasmonic crystals. Under excitation at frequency ω, the third order susceptibility $\chi^{(3)}$ of a material induces a nonlinear polarization $\mathbf{P}^{(3)}(3\omega)$ defined by:

$$\mathbf{P}^{(3)}(3\omega)= \varepsilon_0 \chi^{(3)}(3\omega; \omega, \omega, \omega)E(\omega) E(\omega) E(\omega). \quad (1)$$

For all experimental measurements performed in this study, the incident wavelength delivered by a collinear optical parametric amplifier (pulse duration 140 fs, repetition rate 100 kHz) was set at λ_{inc}= 1500 nm, corresponding to a third harmonic generation centered at λ_{THG}= 500 nm. The third harmonic responses from the hybrid and bare plasmonic crystals excited under parallel polarized excitation were quantified using a standard spectrometer (PI Acton SP2300, Princeton Instruments) for an incident average excitation power of 15 μW. Results are presented in **Figure 2a**. We point out that SiO_2 material was chosen as substrate due to its low third order susceptibility ($\chi^{(3)}_{SiO2} = 2.5 \times 10^{-22}$ m^2/V^2 [27]). Therefore its contribution on the

detected nonlinear signal can be neglected, as preliminary FDTD simulations confirmed using $\chi^{(3)}_{SiO2} = 0$ and 2.5×10^{-22} m^2/V^2. The integration of the spectroscopic curves provides a direct access to the overall third harmonic intensity, and leads to values of 1.2×10^5 photon.s^{-1} and 2.1×10^4 photon.s^{-1} for the hybrid and bare plasmonic crystals respectively. From these data, we determined a significant 6 times enhancement of the raw third harmonic signal for the hybrid ITO plasmonic crystal compared to that of the bare plasmonic crystal. In addition, we plotted in **Figure 2b** the evolution of the third harmonic conversion for increasing excitation power for the hybrid and bare plasmonic crystals. As expected, a numerical fit of the spectroscopic data shows that the THG signal grows cubically with the incident fundamental intensity for both configurations. In order to predict whether it would be possible to reach larger third harmonic signal using different materials for the hybrid crystal, the origin of the enhancement mechanism has to be unveiled. Recently, independent third harmonic experiments on such hybrid ITO plasmonic nanostructures have shown that the main contribution in the nonlinear signal was related to the active nonlinear medium (ITO) or to the bare plasmonic nanostructure itself, leading to different interpretations on the nature of nonlinear interactions at the nanoscale[23,24]. To further investigate the respective contribution of the plasmonic metal and the nonlinear active medium on the third harmonic signal, we will introduce below a new characterization method based on a combination of experiments and numerical simulations, and conclude that the nonlinear response generated by hybrid plasmonic nanostructures contains a unique spectral fingerprint regarding the origin of the signal.

In order to isolate the origin of the THG unambiguously, we will focus hereafter on a single cell of the hybrid and bare plasmonic crystal as presented in the SEM images in **Figure 3a,b**. This single dimer configuration provides a simpler situation. This approach is justified in light of the numerically-computed intensity enhancement maps from **Figure 3c,d**, which are

similar to those shown in Figure 1c,d for the crystal configuration. Experimental THG spectra from 35 nm gap nanorod dimers with and without an ITO nanoparticle at their gaps excited with an incident average power of 50 μW under parallel polarization are presented in **Figure 3e**. As can be seen, the third harmonic light from the hybrid ITO-plasmonic dimer is one order of magnitude brighter (1.4×10^5 photon.s^{-1}) than the light from the bare plasmonic dimer (10^4 photon.s^{-1}) leading to an overall THG enhancement of 14, in good agreement with the value obtained with the hybrid ITO plasmonic crystal. Depending on the physical mechanisms responsible for the THG enhancement, one can expect variations in terms of radiative damping for the hybrid compared to the bare configurations, as the semiconductor and metallic materials exhibit different linear and nonlinear properties. As reported in previous works[28], a qualitative estimation of the damping can be provided via a temporal or spectral analysis of the third harmonic response. Therefore, the experimental THG spectra of the nanostructures presented in Figure 3e under parallel polarized excitation were normalized by their respective maximum intensities in **Figure 3f**. From these data, it appears that the shape of the nonlinear spectra presents significant differences in terms of linewidth. Indeed, the third harmonic spectrum determined for the hybrid ITO plasmonic dimer is surprisingly compressed compared to the bare plasmonic dimer. This spectral compression can be quantified in terms of full-width at half-maximum (FWHM), leading to a FWHM reduction of the hybrid nanodimer's spectrum by 17% compared the bare nanodimer's spectrum. Such peculiar phenomenon is directly correlated to a higher third harmonic damping rate $\Gamma \propto 1/\mathrm{FWHM}$[28], as the ITO nanoparticle is located in an area of strong interactions in terms of field enhancement and nonradiative emission[29].

In order to corroborate these experimental observations, FDTD nonlinear simulations (see Experimental Section) were performed for determining the third harmonic spectra from the plasmonic nanorod dimer with and without an ITO nanoparticle at its gap. Normalized results

are presented in **Figure 3g** and the polarization of THG signal for the hybrid nanodimer is available in the Supplementary Information. Notice that we numerically investigated the cases when the ITO material of the hybrid configuration is considered linear ($\chi^{(3)}_{ITO} = 0$) or nonlinear ($\chi^{(3)}_{ITO} = 2.16 \times 10^{-18}\ m^2/V^2$ [26]) while gold is considered always nonlinear ($\chi^{(3)}_{Au} = 7.6 \times 10^{-19}\ m^2/V^2$ [27]). Alike the experimental data, the numerical work shows that the third harmonic linewidth of the bare plasmonic configuration is larger than that of the hybrid nanostructure when considering the ITO material nonlinear, while the hybrid and bare nanostructures exhibit identical spectra (despite the fact that these two systems are geometrically distinguished) when ITO is considered linear. In regards to these numerical data, we believe that the nonlinear damping in the hybrid nanostructure (when ITO is considered linear) is not modified compared to its bare plasmonic configuration because the dielectric material at the gap does not introduce non radiative perturbations in the third harmonic generation process occurring in the metallic structure. When the ITO material is considered nonlinear, the FWHM of the hybrid nanodimer's spectrum is reduced by 15% compared the bare nanodimer's spectrum, in good agreement with the experimental observations. This confirms that the overall nonlinear enhancement in such hybrid configurations originates from the plasmon-enhanced ITO third harmonic emission. Interestingly, this nonlinear compression is also highlighted in the normalized THG spectra of the hybrid ITO plasmonic crystals presented in **Figure 3h**. The FWHM spectral compression for the hybrid crystal is about 15% compared to the bare crystal, thus indicating that the overall THG enhancement originates from the ITO nanoparticle. Therefore, we can expect that using an active nonlinear medium with higher intrinsic third order susceptibility would lead to stronger THG response from the hybrid crystal. This is further discussed in the Supplementary Information where $\chi^{(3)}_{ITO} = \chi^{(3)}_{Au}$ is studied.

To extend this nonlinear characterization method in the framework of other plasmonic designs, we investigated another experimental configuration made by a 30 nm and 55 nm gap nanocylinder dimer with and without an ITO nanoparticle at their gaps (**Figure 4a,b**). The experimental third harmonic generation spectra for both configurations determined for both configurations with an incident average excitation power of 50 μW and under parallel polarization are presented in **Figure 4c,d**. From this data, we can conjecture that the enhanced THG signal achieved with the hybrid 30 nm gap nanocylinder dimer may be originated from the semiconductor material. However, in the case of the ITO nanoparticle coupled to the 55 nm gap nanocylinder dimer, it is apparent that the nonlinear signal cannot be related to the semiconductor material, as the third harmonic emission for the hybrid configuration is weaker than the signal measured for its corresponding bare metallic configuration. On the other hand and while one can expect that a higher THG signal should be provided with a bare 30 nm gap nanocylinder dimer (Figure 4c), we experimentally determined a slightly higher THG signal with the bare 55 nm gap configuration (Figure 4d). We believe that these observations are related to experimental uncertainties such as fabrication (shape of the nanodiscs, roughness of the metal...) and measurements (lower signal to noise ratio compared to the nanorod comfiguration, excitation wavelength out of the peak resonance, and fluctuation of the laser power...). As for the nanorod dimer's configuration, the experimental observations are further confirmed by the spectral analysis of the third harmonic signal in **Figure 4e,f**, in which the experimental nonlinear spectra presented in Figure 4c,d have been normalized by their respective maximum intensities. As remarkable, the normalized nonlinear signal for the 30 nm gap nanocylinder dimer with and without an ITO nanoparticle at its gap present variations in terms of spectral width, comparable to the nanorod configuration of the Figure 3b. From these data, we determined an experimental FWHM compression of 9% for the hybrid compared to the bare 30 nm gap nanorod dimer. Nevertheless, the normalized nonlinear spectrum of the hybrid 55 nm nanocylinder does not exhibit any particular modification in

terms of FWHM, thus corroborating the assumption that in this case, the nonlinear signal from the hybrid nanostructure originates from the metal's contribution.

We give support to these findings by computing numerically the normalized third harmonic spectra of the 30 nm and 55 nm gap hybrid and bare configurations in **Figure 4g,h** respectively. The polarimetric analysis of the THG is shown in the Supplementary Information. Here again, we investigated the cases when the ITO material of the hybrid configuration is considered linear or nonlinear, while gold is considered nonlinear. Focusing first on the 30 nm gap nanocylinder dimer configuration (Figure 4g), we determined a simulated FWHM compression of 11% when considering ITO as nonlinear (in agreement with the experimental value of 9%), while no simulated spectral compression is observed when the ITO material is considered linear. By combining the results presented in Figure 4c,e,g, we conclude that the overall nonlinear enhancement occurring with the hybrid 30 nm gap nanocylinder dimer is related to the plasmon-enhanced third harmonic ITO effect. Focusing now on the 55 nm gap nanocylinder dimer (Figure 4h), we determined a FWHM compression of about 12% when considering ITO as nonlinear, while no spectral compression was experimentally observed (Figure 4f), leading to a discrepancy in terms of experiments-simulations comparison. Such discrepancy is directly related to what concerns related to the results presented in Figure 4d, i.e. to the fact that for this configuration, the THG signal does not originates from the ITO nanoparticle. In order to take into account this experimental observation, we have also simulated in Figure 4h the hybrid spectrum when considering ITO as linear (which is equivalent to assume that the THG signal originates from the metallic part of the hybrid configuration) as well as the simulated spectrum for the bare metallic configuration. As can be seen in Figure 4h, the simulated hybrid spectrum when considering ITO as linear is similar to the simulated spectrum determined for the bare metallic configuration. Therefore, from results presented in Figure 4d,f,h, we deduce that when the gap is increased from 30 to 55 nm, the experimental THG signal from the hybrid nanocylinder

dimer is not related to the semiconductor anymore, but to the metal contribution (see Supplementary Information for more discussion). Such observation is a direct consequence of the fast decrease of the third harmonic signal for increasing plasmonic dimers' gaps. Indeed, as the THG from the ITO nanoparticle is sensitive to the cubic fundamental intensity at the gap of the dimers, the third harmonic light generated by the ITO nanoparticle is not bright enough to overcome the nonlinear background from the bare nanocylinder dimer for large gaps. This leads to only measure the intrinsic third harmonic contribution from gold when the gap of the hybrid nanocylinder dimer is increased from 30 to 55 nm, and further reinforces our point that the spectral compression is univocally linked to the third harmonic process undergone within the ITO nanoparticle.

In conclusion, we reported the fabrication and characterization of a hybrid crystal made by a combination of semiconductor and metallic materials for enhancing third harmonic generation of light. The origin of the signal was determined by introducing a new characterization method on a single cell of the crystal. We demonstrated that a rigorous combined experimental and numerical FWHM analysis of the nonlinear spectra from a hybrid nanostructure and its bare plasmonic configuration may enable to unveil the origin of the third harmonic signal. Indeed, as the third harmonic emission is affected by a specific damping rate in each case, the width of the third harmonic spectrum exhibits noticeable variations whether the signal originates from the semiconductor or metallic material. This unique spectral fingerprint helps identify the origin of the nonlinear signal at the nanoscale with a far-field method. Further investigations with excitation pulse lengths below 10 fs (i.e., comparable to the plasmon lifetime) as described in Reference[28] would be interesting to infer more physical insight on the problem (since the former measurements would enable time-resolving the plasmonic effect) and corroborate the conclusions that we drew from a solid combination of numerical and experimental studies using a 150 fs pulse. Notice that the THG is an instantaneous process and cannot be time-resolved with fs lasers. We believe these results

open new opportunities for tracing the nature of the nonlinear interactions at the nanoscale and optimizing the harmonic responses in complex hybrid nanodevices.

Experimental Section

Nanofabrication: The hybrid plasmonic nanostructures presented in this work were fabricated by rigorous combination of etch-down and lift-of methods. Briefly, sputtering deposition was used to cover a quartz substrate with a 40 nm ITO film. Nanodots were then defined in HSQ resist by e-beam lithography followed by ion beam etching of the ITO layer in order to generate arrays of ~25-35 nm ITO particles. Hereafter, the quartz substrate was coated with PMMA resist in which the nanorods array shapes were defined around the ITO nanodots and covered with a 2 nm Cr adhesion layer and a 40 nm Au film by thermal evaporation. A final lift-off step leads to the hybrid nanostructures presented in Figure 1a,b.

Experimental measurements: Experimental measurements were carried out on a custom nonlinear inverted microscope. The excitation was performed by a collinear optical parametric amplifier OPA (ORPHEUS OPA with LYRA wavelength extension option, Light Conversion Ltd, Lithuania, pulse duration 140 fs, repetition rate 100 kHz) pumped by a Yb:KGW femtosecond PHAROS laser system. The fundamental incident beam at λ_{inc}= 1500 nm (excitation power set below 50 μW corresponding to a peak intensity of 3.4 kW in order to prevent sample damage) was reflected by a shortpass dichroic mirror and focused on the sample plane by a dry microscope objective (Nikon S Plan Fluor ×40, 0.6 NA). The backward-emitted third harmonic generation at λ_{THG} = 500 nm was collected via the same microscope objective and directed to a 70:30 cube beam splitter that separates the light towards a spectrograph (PI Acton SP2300, Princeton Instruments) or towards an avalanche photodiode (MPD PDM Series, Picoquant). The nanopositioning of the sample at the laser focus spot was ensured by a multiaxis piezoelectric stage (Nano-Drive, Mad City Labs).

Numerical simulation: We performed three-dimensional finite-difference time-domain (FDTD) simulations using the commercial software FDTD Solution v8.9.173 (Lumerical).

Linear and especially non-linear simulations of plasmonic structures are computationally intensive. Hence, the computation demand was reduced by considering the dimers (whose long and short axes are along *x* and *y*, respectively) as two ideal rectangles or discs, and the ITO particle as a perfect disc placed at the centre of the gap (which is the origin of the coordinate system). This allowed us to use a twofold symmetry [i.e., electric, $E_t = 0$, (software-defined anti-symmetric) and magnetic, $H_t = 0$, (software-defined symmetric) walls (boundaries) on the $x = 0$ and $y = 0$ planes, respectively]. We point out that because of the strong coupling between neighbouring nanorods for the crystal configuration, we choose to trace the origin of the nonlinear signal by deriving the information from a single cell of the crystal (isolated hybrid nanostructure) and translating the information to the array constituting the hybrid crystal. For the linear simulations of the crystal, the boundary conditions in x_{max} and y_{max} were set to electric and magnetic walls, respectively, whereas the boundary conditions along *z* were set as perfect matched layers. With these boundaries, we model an infinite array along *x* and *y*, over a semi-infinite substrate. The excitation was done via a plane-wave polarized along *x* (i.e., parallel). For the linear and nonlinear simulations of single dimers, all simulation boundaries were set as perfect matched layers to model a single dimer over a semi-infinite substrate. To further reduce the computation effort, the solver-defined total-field scattered-field (TFSF) source was used to define a plane-wave excitation only within the volume enclosing the dimer.

The dimensions of the dimers were estimated from scanning electron microscopy (SEM) images of the fabricated dimers such as the one presented in Figure 1a,b, Figure 3a,b and Figure 4a,b and were rounded to realize the twofold symmetric ideal geometries. Namely, the length × width × height (notice that the height corresponds to the metal thickness) of each nano-dipole's arm was 320/280 nm × 100 nm × 40 nm for the crystal/single dimer. Meanwhile, the diameter and height of the discs comprising the disc dimer was 290 nm and 40 nm, respectively. The Cr adhesion layer had the same geometry as the dimer but a thickness of 2

nm. The gap of the nanorod dimer was 35 nm, and the ITO disc had a diameter and height of 35/20 nm and 45 nm, respectively for the crystal/single dimer. The gap of the nanodisc dimers was 30 and 55 nm, whereas the ITO disc had for these two cases a diameter and height of 25 nm and 45 nm, respectively.

The dielectric linear dispersion of Au, and Cr (adhesion layer) was fitted within the spectral range 400 nm – 2000 nm to tabulated data[30] with a multi-coefficient function (allowing a tolerance of 0.1 and enforcing passivity), whereas the lossless SiO_2 (semi-infinite substrate) and ITO linear property was modelled as a constant permittivity of 2.122 and 2.890, respectively[30,26]. The nonlinear response of Au and ITO was considered by incorporating to the base linear function the intrinsic $\chi^{(3)}_{Au} = 7.6 \times 10^{-19}\,m^2/V^2$ and $\chi^{(3)}_{ITO} = 2.16 \times 10^{-18}\,m^2/V^2$, respectively [27,26]. The nonlinear response of SiO_2 was not considered for this manuscript to alleviate computational effort. This is a good approximation in the light of a preliminary simulation considering $\chi^{(3)}_{SiO2} = 2.5 \times 10^{-22}\,m^2/V^2$ [27], which showed a variation of only 4% in the third harmonic intensity compared to $\chi^{(3)}_{SiO2} = 0$.

A conformal non-uniform mesh was used to accurately map the hybrid structure geometry and model its electromagnetic properties. The unit cell of the crystal has dimensions 355 nm $\times$ 300 nm $\times$ 4000 nm and the default grid was 6 nm $\times$ 6 nm $\times$ 3 nm. The gap region was discretized by default with a cubic grid of 2 nm $\times$ 2 nm $\times$ 1.5 nm, but the region enclosing the ITO cylinder had a cubic grid of 0.5 nm $\times$ 0.5 nm $\times$ 1.5 nm. A finer mesh along *z* of 0.5 nm was applied for the Cr adhesion layer. The simulation stopped when the residual energy in the calculation volume was at least 1×10^5 of the maximum energy injected. A standard convergence test was performed to ensure negligible numerical errors originating from the perfect matched-layer distance, non-uniform meshing or monitor sampling.

For the single dimer configuration, the TFSF volume had dimensions of 800 nm $\times$ 400 nm $\times$ 80 nm and the default grid was 7 nm $\times$ 7 nm $\times$ 3 nm. For the gap region, the volume with

dimensions 120 nm × 140 nm × 50 nm was discretized with a cubic grid of 2.5 nm × 2.5 nm × 1.5 nm. An even smaller cubic grid of 0.3 nm × 0.3 nm × 1 nm was overridden in the region enclosing the ITO cylinder. A finer mesh size along *z* of 0.5 nm was applied for the Cr adhesion layer. The *x*-polarized plane-wave excitation was incident normal to the dimer, and had an amplitude of 1×10^8 V/m and 2×10^8 V/m for the rod and disc dimer, respectively, chosen to satisfy the condition $\chi^{(3)}|E(t)|^2 << \varepsilon_r$, where $\chi^{(3)}$ and ε_r are the third-order susceptibility and electric permittivity of Au or ITO, and E(t) is the temporal induced electric field in Au or ITO (the non-linear materials). This excitation was a realistic narrowband temporal pulse with central wavelength of 1500 nm and spectral width ~23.65 nm (i.e. pulse length of 140 fs). The maximum simulation time was set to 1700 fs. The time stepping stability factor was set to 0.95, which corresponds to a time step of δt = 0.00061 fs. A standard convergence test was also performed for the single dimers.

We follow two different approaches to estimate the spectra at the third harmonic. On the one hand, the spectra is calculated from the total power flowing outward through a plane 40 nm above the dimer and extension 1100 nm × 700 nm. On the other hand, as an additional check, we also recorded the waveform at one top edge of the simulation box and Fourier-transform it to obtain the spectra. Although the latter results are not shown in the manuscript, they are in agreement with those computed via the first method.

Acknowledgements
The authors thank Tasmiat Rahman from the Optical and Semiconductor Devices Group, Imperial College London, for his help during the nonlinear simulations. This work was funded by the Engineering and Physical Sciences Research Council (EPSRC) through the Active Plasmonics programme, the Leverhulme Trust, the US Army International Technology Centre Atlantic (USAITC-A) and the Office of Naval Research (ONR and ONR Global). M.N-C. is supported by an Imperial College Junior Research Fellowship.

Received: ((will be filled in by the editorial staff))
Revised: ((will be filled in by the editorial staff))
Published online: ((will be filled in by the editorial staff))

[1] J. A. Schuller, E. S. Barnard, W. S. Cai, Y. C. Jun, J. S. White, M. L. Brongersma, *Nat. Mater.* **2010**, *9*, 193.

[2] H. A. Atwater, A. Polman, *Nat. Mater.* **2010**, *9*, 205.

[3] M. Rahmani, E. Yoxall, B. Hopkins, Y. Sonnefraud, Y. Kivshar, M. Hong, C. Phillips, S. A. Maier, A. E Miroshnichenko, *ACS Nano* **2013**, *7*, 11138.

[4] P. Bharadwaj, B. Deutsch, L. Novotny, *Adv. Opt. Photonics* **2009**, *1*, 438.

[5] L. Novotny, N. F. van-Hulst, *Nat. Photon.* **2011**, *5*, 83.

[6] A. Kinkhabwala, Z. F. Yu, S. H. Fan, Y. Avlasevich, K. Mullen, W. E. Moerner, *Nat. Photon.* **2009**, *3*, 654.

[7] H. Aouani, O. Mahboub, E. Devaux, H. Rigneault, T. W. Ebbesen, J. Wenger, *Opt. Express* **2011**, *19*, 13056.

[8] D. Punj, M. Mivelle, S. B. Moparthi, T. S. van Zanten, H. Rigneault, N. F. van Hulst, M. F. Garcia-Parajo, J. Wenger, *Nat. Nanotechnol.* **2013**, *8*, 512.

[9] A. Curto, G. Volpe, T. H. Taminiau, M. Kreuzer, R. Quidant, N. F. Van Hulst, *Science* **2010**, *329*, 930.

[10] H. Aouani, O. Mahboub, N. Bonod, E. Devaux, E. Popov, H. Rigneault, T. W. Ebbesen, J. Wenger, *Nano Lett.* **2011**, *11*, 637.

[11] D. Vercruysse, Y. Sonnefraud, N. Verellen, F. B. Fuchs, G. Di Martino, L. Lagae, V. V. Moshchalkov, S. A. Maier, P. Van Dorpe, *Nano Lett.* **2013**, *11*, 3843.

[12] F. Neubrech, A. Pucci, T. W. Cornelius, S. Karim, A. Garcia-Etxarri, J. Aizpurua, *Phys. Rev. Lett*. **2008**, *101*, 157403.

[13] L. V. Brown, K. Zhao, N. King, H. Sobhani, P. Nordlander , N. J. Halas, *J. Am. Chem. Soc*. **2013**, *135*, 3688.

[14] H. Aouani, M. Rahmani, H. Šípová, V. Torres, K. Hegnerová, M. Beruete, J. Homola, M. Hong, M. Navarro-Cía, S. A. Maier, *J. Phys. Chem. C.* **2013**, *117*, 18620.

[15] Y. Zhang, N. K. Grady, C. Ayala-Orozco, N. J. Halas, *Nano Lett.* **2011**, *11*, 5519.

[16] H. Aouani, M. Navarro-Cía, M. Rahmani, T. P. H. Sidiropoulos, M. Hong, R. Oulton, S. A. Maier, *Nano Lett.* **2012**, *12*, 4997.

[17] M. Sivis, M. Duwe, B. Abel, C. Ropers, *Nat. Phys. 2013*, *9*, 304.

[18] T. Schumacher, K. Kratzer, D. Molnar, M. Hentschel, H. Giessen, M. Lippitz, *Nat. Commun.* **2011**, *2*, 333.

[19] M. Kauranen, A. V. Zayats, *Nat. Photon.* **2012**, *6*, 737.

[20] Y. Pu, R. Grange, C.-L. Hsieh, D. Psaltis, *Phys. Rev. Lett.* **2010**, *104*, 207402.

[21] H. Harutyunyan, G. Volpe, R. Quidant, L. Novotny, *Phys. Rev. Lett.* **2012**, *108*, 217403.

[22] M. Navarro-Cía, S. A. Maier, *ACS Nano* **2012**, *6*, 3537.

[23] H. Aouani, M. Rahmani, M. Navarro-Cía, S. A. Maier, *Nat. Nanotechnol.* **2014**, *9*, 290.

[24] B. Metzger, M. Hentschel, T. Schumacher, M. Lippitz, X. Ye, C. B. Murray, B. Knabe, K. Buse, H. Giessen, *Nano Lett.* **2014**, *14*, 2867.

[25] S. Chen, W. Wong, Y. Pun, K. Cheah, G. Li, *Adv. Optical Mater.* **2013**, *1*, 522.

[26] J. L. Humphrey, D. Kuciauskas, *J. Appl. Phys.* **2006**, *100*, 113123.

[27] R. W. Boyd, Nonlinear optics; *Academic Press*, **2008**.

[28] T. Hanke, J. Cesar, V. Knittel, A. Trügler, U. Hohenester, A. Leitenstorfer, R. Bratschitsch, *Nano Lett.* **2012**, *12*, 992.

[29] V. Giannini, A. I. Fernandez-Dominguez, S. C. Heck, S. A. Maier, *Chem. Rev.* **2011**, *111*, 3888.

[30] E. D. Palik, Handbook of optical constants of solids; *Academic Press*, **1985**.

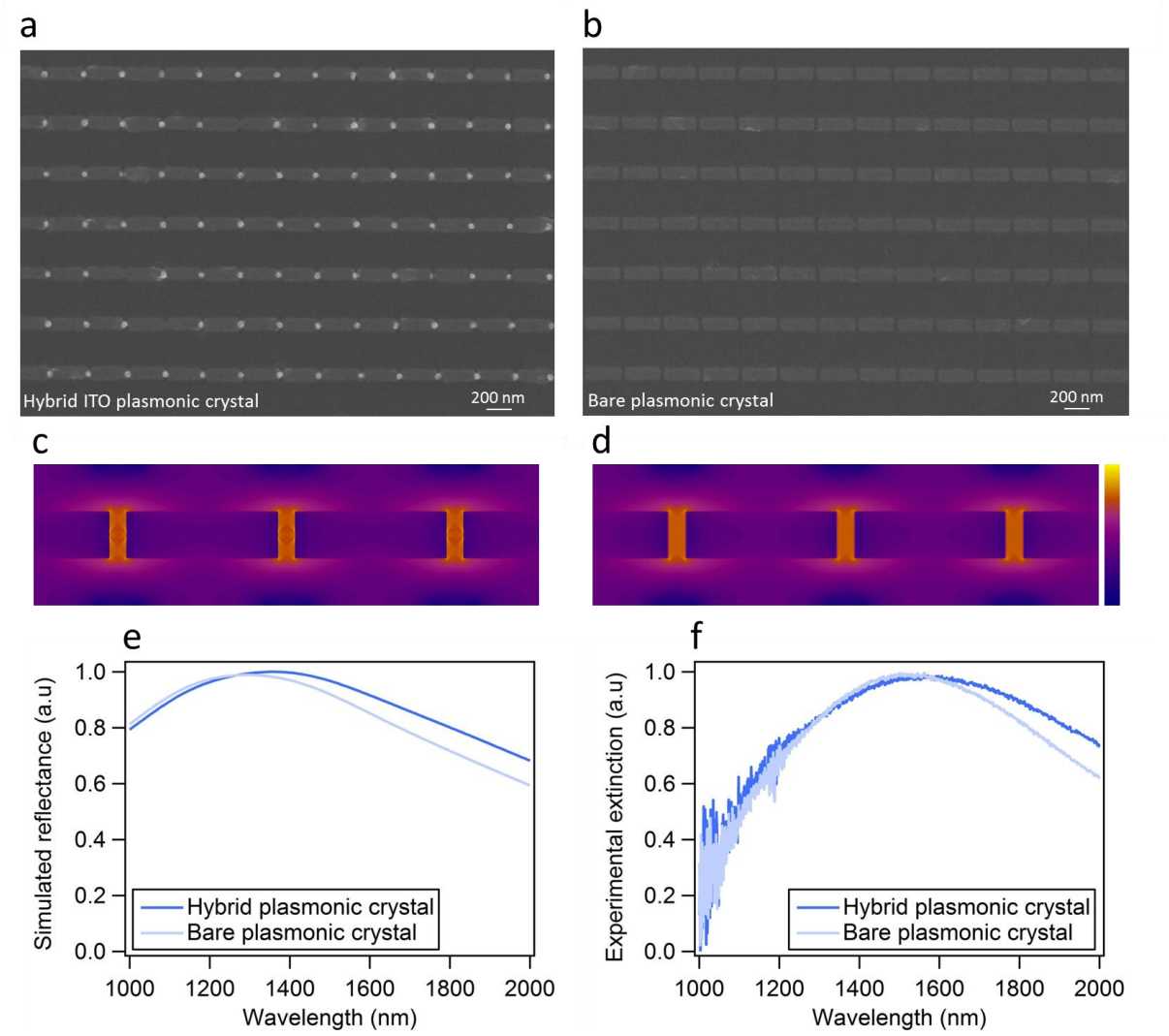

Figure 1. SEM images the hybrid (a) and bare (b) plasmonic crystal. FDTD computation of the intensity enhancement along the middle cross-sectional plane for the wavelength of the reflectance peak from panel (e) corresponding to the hybrid (c) and bare (d) plasmonic configuration. Simulated reflectance (e) and experimental extinction cross section (f) of the hybrid and plasmonic crystal.

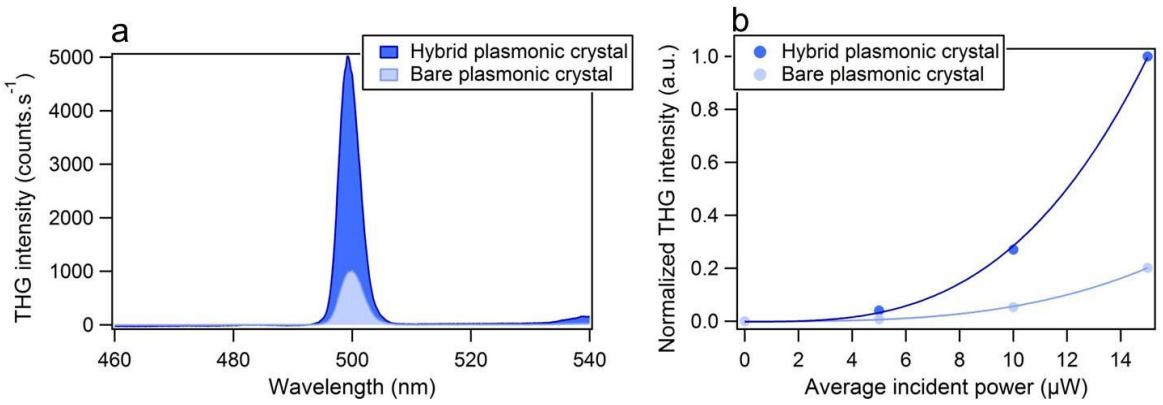

Figure 2. (a) Experimental third harmonic generation spectra of the hybrid ITO and bare plasmonic crystals excited under parallel polarized excitation. (b) Evolution of the third harmonic signal for increasing excitation powers.

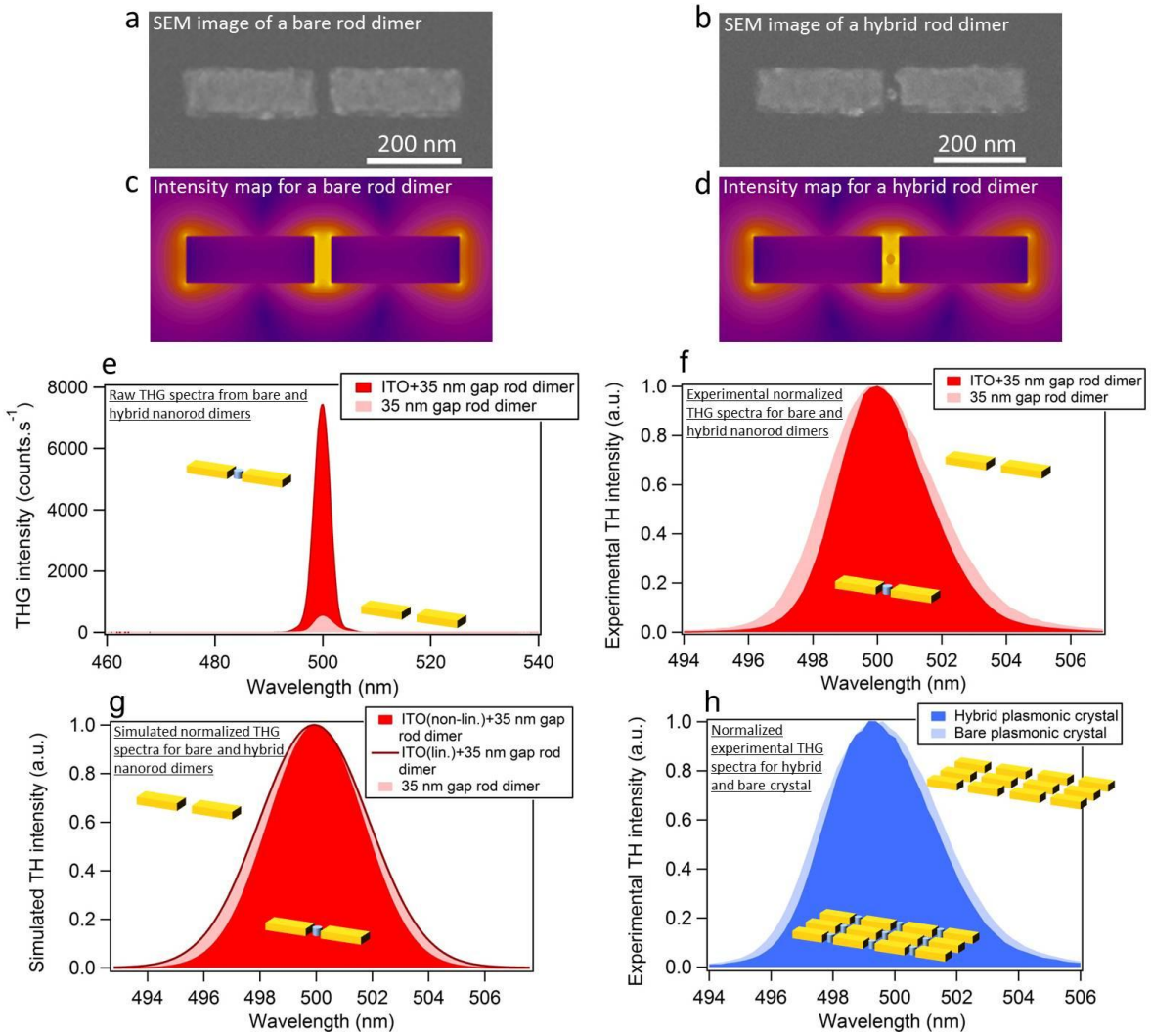

Figure 3. SEM images of a 35 nm gap nanorod dimer without (a) with (b) a ~20 nm ITO nanoparticle at its gap. FDTD computation of the intensity enhancement along the middle cross-sectional plane for λ = 1500 nm and an incident plane-wave under parallel polarization corresponding to a 35 nm gap nanorod dimer without (c) and with (d) a ~20 nm ITO nanoparticle at its gap. (e) Experimental third harmonic generation spectra from the nanostructures presented in (a,b) under parallel polarized excitation. Experimental (f) and simulated (g) normalized third harmonic generation spectra from a 35 nm gap nanorod dimer with and without a ~20 nm ITO nanoparticle at its gap under parallel polarized excitation. Notice that for (g), simulations have been conducted while considering ITO linear ($\chi^{(3)}_{ITO} = 0$) and nonlinear ($\chi^{(3)}_{ITO} = 2.16 \times 10^{-18}$ m^2/V^2) to corroborate the experimental observations. (h) Normalized experimental third harmonic generation spectra from the hybrid ITO and bare plasmonic crystals.

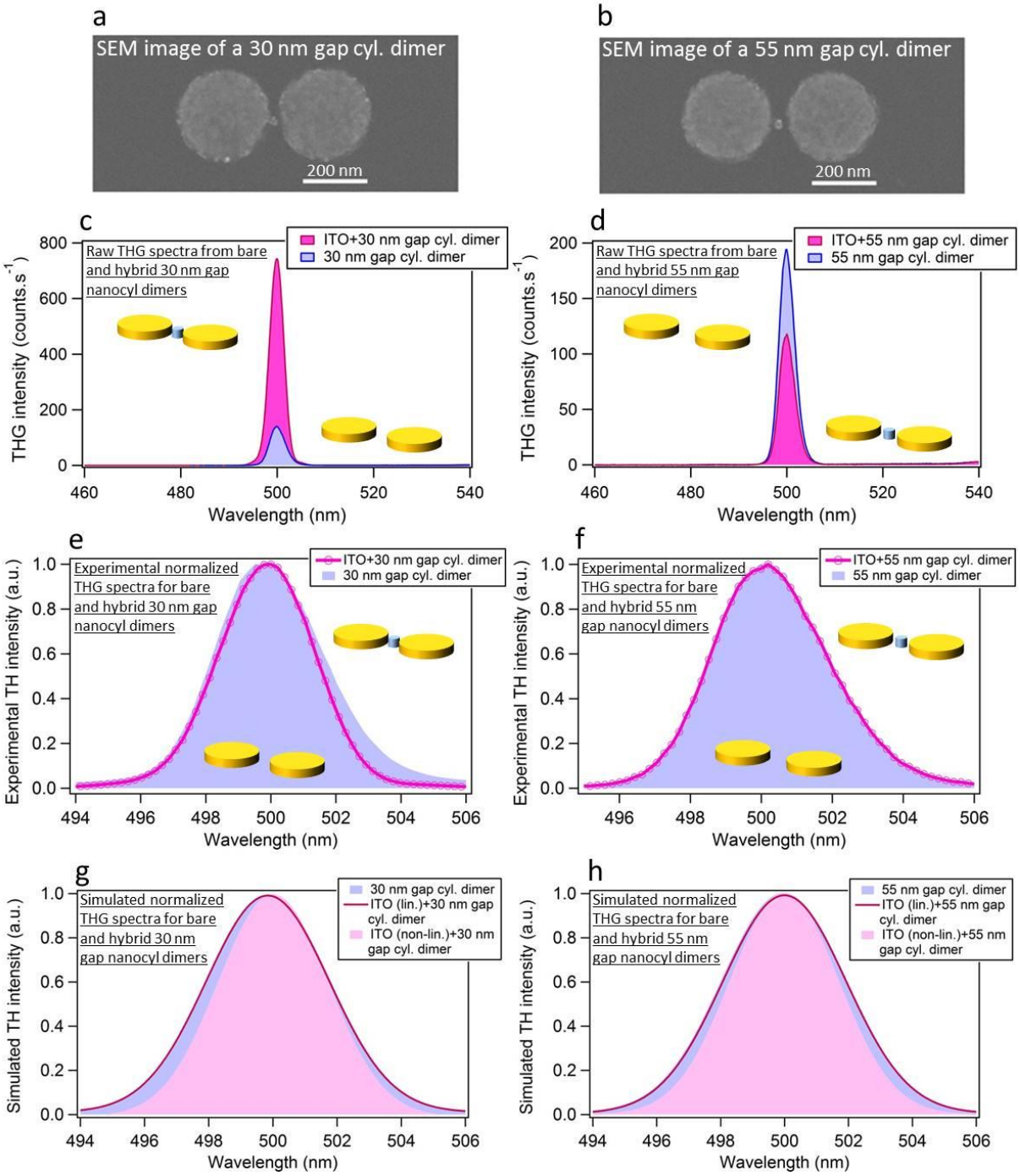

Figure 4. SEM images of a 30 nm (a) and 55 nm gap (b) nanocylinder dimers with a ~25 nm ITO nanoparticle at their gaps. Experimental third harmonic generation spectra from a 30 nm (c) and 55 nm gap (d) nanocylinder dimer with and without a ~25 nm ITO nanoparticle at their gaps under parallel polarized excitation. Normalized experimental spectra of the third harmonic generation signal from the 30 nm (e) and 55 nm (f) gap nanocylinder dimers with and without a ~25 nm ITO nanoparticle at their gap under parallel polarized excitation and normalized numerical spectra (g,h) corresponding to (e,f), respectively. Notice that for (e,f), simulations have been conducted while considering ITO linear ($\chi^{(3)}_{ITO} = 0$) and nonlinear ($\chi^{(3)}_{ITO} = 2.16 \times 10^{-18}\ m^2/V^2$) to corroborate the experimental observations.

Table of content: We propose a hybrid plasmonic crystal for reaching higher nonlinear upconversion rate and we unveil the physical mechanism behind the enhancement by demonstrating that the nonlinear signal contains a unique spectral fingerprint regarding its origin. This opens new opportunities for understanding and optimizing nonlinear light-matter interactions in complex nanoscale media.

Keyword plasmonic crystal, hybrid plasmonic antenna, nonlinear nanophotonics, third harmonic generation, spectral analysis

Heykel Aouani[†], Miguel Navarro-Cía[†], Mohsen Rahmani, and Stefan A. Maier*

Unveiling the Origin of Third Harmonic Generation in Hybrid ITO-Plasmonic Crystals

ToC figure